

Statistical Analysis of the Inclusions in Rare Earth-M ($M = \text{Ca}$ and Ti) Treated Steel



YUMIN XIE, MINGMING SONG, BAO WANG, HANGYU ZHU, ZHENGLIANG XUE, ALEXANDER MAYERHOFER, SUSANNE KATHARINA MICHELIC, CHRISTIAN BERNHARD, and JOHANNES LEOPOLD SCHENK

The size, quantity, morphology and structure of inclusions in steel treated with rare earth (RE) with different deoxidizers (calcium and titanium) were studied. The difference between automatic and manual inclusion statistical analyses was investigated. The results showed that: RE tended to refine the inclusions and increase the number density of the inclusions in steel. When combined with RE, calcium and titanium could reduce the number densities of inclusions. The mean diameters of the inclusions in the RE-treated steel and RE-titanium-treated steel were close, and smaller than that in the RE-calcium-treated steel. Calcium and titanium reduced the mean aspect ratio of inclusions in the RE-treated steel. RE particles and MnS formed random composite inclusions when only RE was added. In RE-calcium-containing composite inclusion, the amount of MnS was very low. For RE-titanium-treated steel, almost all titanium formed composite inclusions with RE. The inclusion automatic analysis (IAA) system showed better performance in counting the content percentage of inclusions. However, for determining the inclusion number in RE-containing steel and size statistical analysis, manual inclusion statistical analysis was superior.

<https://doi.org/10.1007/s11663-021-02163-0>

© The Minerals, Metals & Materials Society and ASM International 2021

I. INTRODUCTION

THE investigation of non-metallic inclusions (NMIs) in steel is a traditional research topic in the field of ferrous metallurgy, and a number of important studies on NMIs have been conducted over several decades.^[1–3] Generally, NMIs are considered to be detrimental to the properties of steel.^[4,5] Reducing the size and number of NMIs in steel is an important research topic for

improving the performance of steel products.^[6,7] In particular, NMIs have a strong influence on the mechanical properties and surface quality of pipeline steel.^[8] The strength and toughness of Q690E steel can be significantly improved by decreasing the size of NMIs.^[9] In recent years, it has also been found that NMIs in steel can induce the nucleation of ferrite within the grains of austenite. NMIs act as a nucleus for heterogeneous refining of the microstructure, which is highly beneficial for the properties of steel.^[10] To achieve such refinement, NMIs must have a special composition, size and structure.^[11] However, due to the variety of steel compositions, as well as differences in melting temperatures and alloying methods and uncertainties such as the narrow component control of deoxidizing elements, the precipitation of NMIs is very complicated.^[12,13] Therefore, work to clarify NMI formation is still needed.

Rare earth (RE) has been widely used to improve the properties of steel.^[14] Liu noted that 0.0047 wt pct RE could significantly improve the low-temperature impact toughness of B450NbRE steel.^[15] Additionally, REs such as Ce, La and Nd, can easily modify the chemical composition and morphology of NMIs.^[16] These studies indicated that RE have important application potential in improving steel performance. However, due to their extremely strong chemical activity, REs are usually added to steel with other elements, such as Al and Ca.^[17]

YUMIN XIE, MINGMING SONG, BAO WANG, HANGYU ZHU, and ZHENGLIANG XUE are with the State Key Laboratory of Refractories and Metallurgy, Wuhan University of Science and Technology, Wuhan 430081, China and also with the Key Laboratory for Ferrous Metallurgy and Resources Utilization of Ministry of Education, Wuhan University of Science and Technology, Wuhan 430081, China. Contact E-mail: smma987@163.com ALEXANDER MAYERHOFER, SUSANNE KATHARINA MICHELIC, CHRISTIAN BERNHARD, and JOHANNES LEOPOLD SCHENK are with the Chair of Ferrous Metallurgy, Montanuniversität Leoben, Franz-Josef-Straße 18, 8700 Leoben, Austria.

Manuscript submitted August 26, 2020; accepted March 25, 2021.

Article published online April 29, 2021.

Previous research^[18] found that Ca-Mg-RE-Zr treatment could transform large MnS into small composite NMIs of Ca-Mg-RE-Zr that were evenly dispersed in high-strength steel. Cao noted that Ca-Al NMIs could be modified into finer REAlO₃ in X70 pipeline steel after treatment with Al-Ti-0.05 wt pct RE.^[19] However, additional investigation of the formation of NMIs in steel after the treatment of REs with other elements are still needed. This work systematically studied changes in the number, size, composition and structure of NMIs after titanium and calcium were compounded with RE (La). The present work is an important reference for research on the formation of NMIs in RE treated steel.

II. MATERIAL AND METHODS

A. Material

Four steel samples were melted by a vacuum high-frequency induction furnace with a magnesite lining. The composition of the raw metal was C-0.16 wt pct, Si-0.30 wt pct, Mn-1.50 wt pct, P-0.03 wt pct, S-0.012 wt pct, O-0.0062 wt pct, soluble Al <0.003 wt pct, N-0.0064 wt pct, and Fe-Bal. The ingredients of the melted steel were adjusted by appropriate ratios of alloy at approximately 1600 °C (1873 K). Amorphous pure silicon, sponge titanium and SiCa (30 wt pct Ca) alloy were first added to the melts in sequence to modify the composition of the molten steel. Five minutes later, pure RE metal was added. After smelting, the steel was poured into an ingot mold inside the vacuum furnace and air cooled to room temperature.

Ingot were soaked at 1200 °C (1473 K) in a furnace for 3 hours to homogenize the composition. Then, the ingots were rolled into plates with a thickness of 15 mm. This process began at 1200 °C (1473 K) and finished at 900 °C (1173 K). After rolling, the plates were air cooled to room temperature. Sample were obtained from the rolled plates to investigate the composition of the steels. The Si, Ca, Ti, and RE contents in the steel were analyzed by the inductively coupled plasma atomic emission spectrometry (ICP-AES) method. The O and N contents were obtained by the infrared absorption method. The compositions of the steels are shown in Table I. It should be noted that although the amounts of the RE added to steels 2, 3 and 4 were the same, due to the different purification effects of Ca and Ti on steel, different yield ratios of RE were obtained, leading to different RE concentrations.

B. Methods

Specimens for inclusion analysis with the dimensions 10 × 10 × 10 mm³ were obtained from the steel plates at the center of thickness and one quarter of the width. The position and direction of the sample are shown in Figure 1. Face **a**, parallel to the rolling direction (RD) on the sample, was the testing face. A standard metallographic specimen was obtained after grinding and mechanical polishing. Scanning electron microscopy (SEM) and energy dispersive spectrometry (EDS) were used to observe the NMIs in the samples.

An inclusion automatic analysis (IAA) system attached to the SEM was used to statistically analyze the inclusions in the samples. To date, IAA has been increasingly used.^[20–30] Two different analytical principles were used in IAA system. The first one is the use of EDS spectra for a point-by-point determination of the location and composition of the NMIs in the whole visual field. A region with a composition that differed from that of the matrix was identified as an NMI, and a location that had a composition that differed from that of this NMI was considered a new NMI. The other IAA analytical principle was to identify an NMI based on the contrast under the backscatter mode of SEM followed by the use of EDS for point-by-point determination of the composition of NMIs. Locations with different compositions are considered to be different NMIs. In other words, for both analytical principles, NMIs were determined based on compositional differences. IAA has the following advantages: a large statistical area, the high accuracy of the statistical data, and the comprehensive nature of the NMI information. Therefore, IAA has been favored by a large number of researchers in the fields of materials and metallurgy. In this work, an IAA system attached to a JEOL 7200F SEM was used to statistically analyze the inclusions in the samples. Aztec IAA software produced by Oxford was used to statistically analyze the NMIs. The IAA system parameters

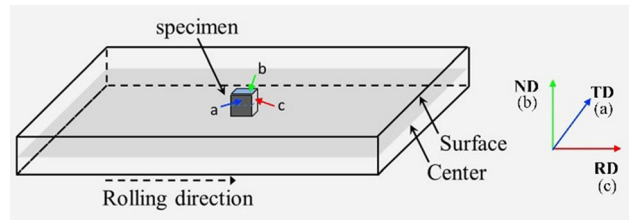


Fig. 1—Position and direction of sampling, RD rolling direction, ND normal to the RD, TD transverse to the RD.

Table I. Composition of the Experimental Steel Samples (Weight Percent)

Sample	C	Si	Mn	P	S	O	N	RE	Ti	Ca	Fe
Steel 1	0.16	0.30	1.50	0.025	0.012	0.0072	0.0074	—	—	—	bal.
Steel 2	0.16	0.33	1.50	0.025	0.012	0.0031	0.0081	0.005	—	—	bal.
Steel 3	0.16	0.31	1.50	0.025	0.012	0.0022	0.0076	0.028	—	0.001	bal.
Steel 4	0.16	0.36	1.50	0.025	0.011	0.0021	0.0075	0.012	0.013	—	bal.

used in this paper are shown in Table II. The IAA measurements were carried out according to GB/T 30834.^[31]

Manual statistics were obtained by SEM under backscatter mode. Sixty images were obtained randomly, and the total statistical analysis area on the test surface of specimens was approximately 1.71 mm². Then, Image J software was used to individually analyze the number and size of NMIs.

Electrolytic extraction of inclusions was carried out using 10 pct AA (10v/v pct acetylacetone-1w/v pct tetramethylammonium chloride-methanol) electrolyte, and the electrical parameters were as follows: 50 to 60 mA and 2.7 to 3.5 V. After filtration of the electrolyte, the morphology of the extracted NMIs was investigated by SEM. The types and quantities of inclusions in each steel under equilibrium were calculated by software using the FTstel database.

Table II. The Parameters of IAA System

Items	Parameters
SEM	JEOL 7200F
EDS Detector	80 mm ² (Oxford) SDD
Beam Energy	15 keV
Working Distance (for EDS)	10 mm
Resolution	2048 px
Min. Particle Size	9 px
Resulting ECD Range	0.3 μm – max
EDS Measurement Time	3 s/feature

III. RESULTS

A. Morphology of NMIs

The morphology and composition of NMIs in the four steel samples are shown in Figure 2. The NMIs were mostly present in the form of composite inclusions. In steel 1, the NMIs were composed of Mn-Si-O and MnS. The NMIs in steel 2 showed two types of contrast. The bright regions were RE-Si-O, and the other regions were Mn-Si-S. The NMIs in steel 3 showed three contrasts. The EDS results showed that the composition of the bright region was RE-S-O, that of the gray region was RE-S-Ca, and that of the dark region was Mn-S-Ca. In steel 4, there were four types of contrasts in one RE composite NMI, corresponding to RE-S-O, RE-Si-S-O, MnS, and TiN in order from bright to dark. The aspect ratios of NMIs in steels 1 and 2 were higher than those of NMIs in steels 3 and 4. The shapes of the NMIs in steels 3 and 4 were approximately spherical.

The EDS mapping results of the NMIs in steels 2, 3 and 4 are shown in Figure 3. The Mn-Si-O NMIs in steel 2 were distributed around the RE-Si-O particles. Some MnS was also present on the surface of steel 2. In steel 3, which had been treated by RE-Ca, the RE regions in the NMIs became cavities. The RE regions were composed of RE-S-O and RE-S-Ca. They were tightly attached, and an Mn-S-Ca layer formed in the gap between the RE-S-O and RE-S-Ca. The structure of the NMIs in steel 4 treated by RE-Ti was relatively complex and irregular. A massive block of RE-S-O and

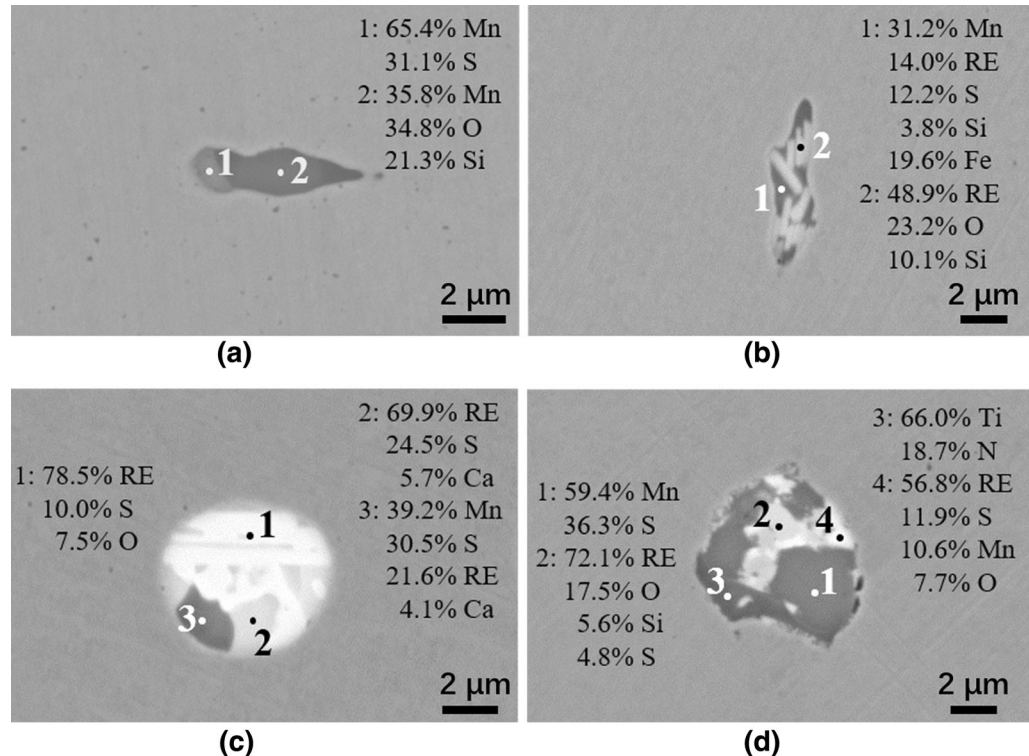


Fig. 2—Morphology and composition of typical NMIs in each steel sample: (a) steel 1; (b) steel 2; (c) steel 3; (d) steel 4. The horizontal direction of (a) and (c) is RD, and the vertical direction of (b) and (d) is RD.

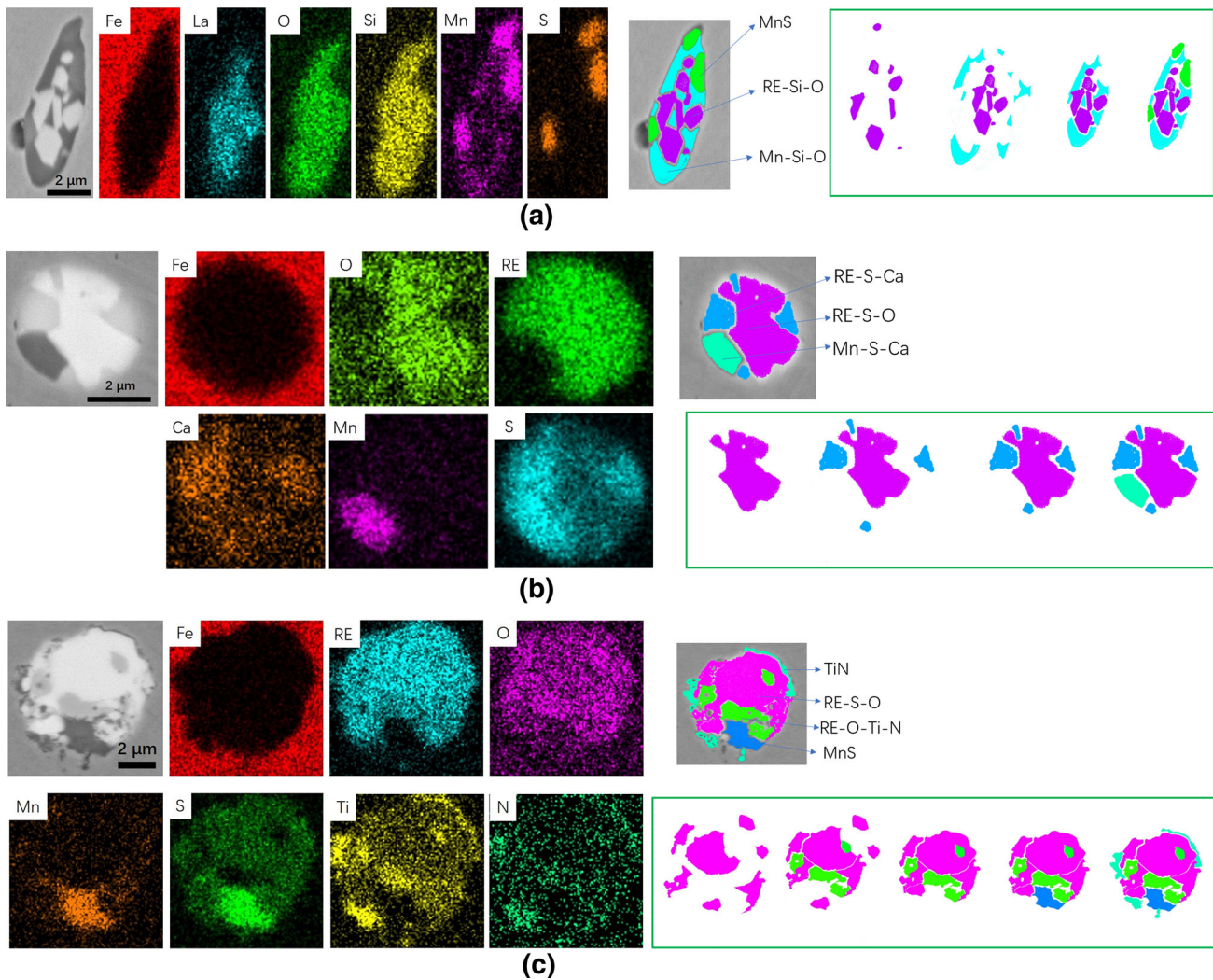


Fig. 3—Component surface distribution of typical NMIs in each steel sample: (a) steel 2; (b) steel 3; (c) steel 4. The vertical direction of (a) is RD, and the horizontal direction of (b) and (c) is RD.

RE-O-Ti-N was observed in the center of the composite NMIs. MnS and TiN comprised the outermost layer and were attached to the surface of the composite NMIs.

Figure 3 shows that the structures of the composite NMIs in steel 3 and 4 were very complex. The morphology of the NMIs in steels 3 and 4 after the electrolytic extraction of NMIs by matrix dissolution is shown in Figure 4. For the NMIs in steel 3, the brighter RE-containing region had a hollow structure, indicating a complex structure. Meanwhile, in steel 4, the NMIs were a solid particle.

B. Statistical Analysis of NMIs

The results of statistical analysis of the number and size of NMIs counted manually and obtained by IAA are shown in Table III. In the IAA analysis, all NMIs containing RE were identified as RE-containing NMIs. In contrast, during the manual statistical process, NMIs with bright or gray regions inside were considered RE-containing NMIs.

The aspect ratios of NMIs in the four steels obtained by manual analysis are shown in Table IV. The aspect ratio of the NMIs after RE treatment was clearly reduced from 3.5 to 1.9. The mean aspect ratio of the NMIs in steel 3 was further reduced to 1.5, which was the smallest ratio. For steel 4, which had been treated with RE-Ti, the mean aspect ratio of the NMIs was approximately 1.8, which was between those upon the RE and RE-Ca treatments.

C. Calculated Results of NMIs

In this study, the steel samples were maintained at 1200 °C (1473 K) for 3 hours before deformation, and the composition and size of NMIs may have changed during the holding process.^[32,33] Because the main NMIs in the test steels were oxides with high thermal stability, changes in the size, quantity and total amount of NMIs may have been small during the holding process. Ignoring the deviation caused by this process in this work, FactSage thermodynamic calculation

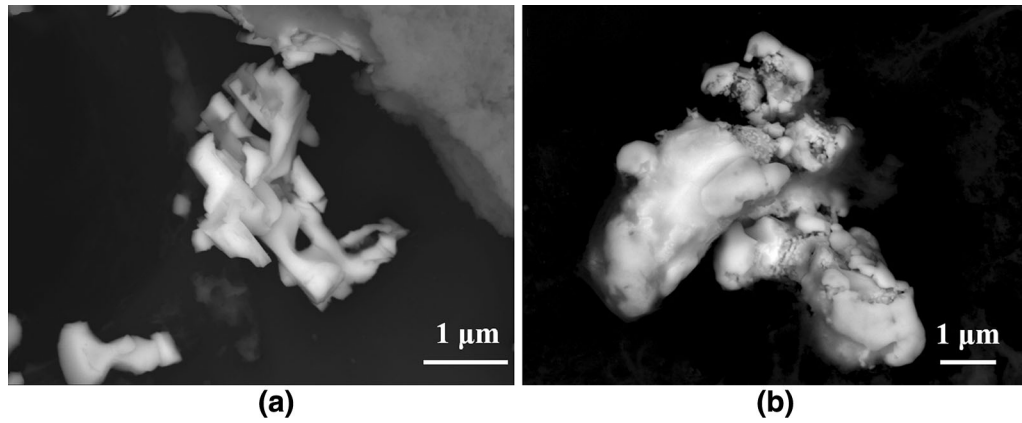


Fig. 4—Backscattering image of the morphology of NMIs in (a) steel 3 and (b) steel 4.

Table III. Statistical Analysis of the Two Methods

	Sample	No. density of all NMI, mm ⁻²	Standard Deviation	No. Density of RE-Containing NMI, mm ⁻²	Standard Deviation	No. Percent of RE-Containing NMI, Pct
Auto ^a	Steel 2	627.3	0.5	319.5	0.6	47.9
	Steel 3	784.2	0.4	596.2	0.7	76.0
	Steel 4	561.6	0.7	271.0	0.3	48.3
Manual	Steel 2	358.0	0.3	56.8	0.9	15.9
	Steel 3	293.0	0.5	200.0	0.3	68.2
	Steel 4	225.0	0.2	90.8	0.7	40.4

^aThe results of analysis are the mean values for three times.

software was used to calculate the types of NMIs during the equilibrium cooling process. The FTstel database was used. The equilibrium calculated contents of different components in all of the NMIs are shown in Table V. All pure RE compounds were regarded as RE NMIs. Similarly, all pure titanium compounds were treated as Ti NMIs. Then, the fraction of the total amount of NMI due to RE NMIs could be easily obtained for the three steels. For steel 4, the sum of the fractions of RE NMIs and Ti NMIs to the total amount of NMIs is also listed in Table V. The fraction of RE NMIs was the highest for steel 3.

IV. DISCUSSION

A. Reasons for the Differences Between the Two Methods

For the purification of melted steel, information about NMI composition, size and quantity is highly important. This information provides important guidance in the steelmaking process to improve the quality of the produced steel.^[34–36] Comparing the two results in Table III, the statistical results with the two methods are quite different. The number densities of NMIs obtained by IAA were significantly higher than those obtained by

Table IV. Aspect Ratio of NMIs in Four Steels

Sample	Mean Aspect Ratio	Biggest Aspect Ratio	Standard Deviation
Steel 1	3.5	17.5	2.4
Steel 2	1.9	10.3	1.1
Steel 3	1.5	9.2	0.6
Steel 4	1.8	7.1	0.9

manual statistics. Then, the backscattering morphology of NMIs in each steel was analyzed, as shown in Figure 5. In steel 1, the contrast of NMIs was lower than that of the matrix, and the contrast difference within a single inclusion was very small. The NMIs in steels 2, 3 and 4 exhibited two or more types of contrast. Some regions had brighter contrast than the matrix, and some showed darker contrast than the base metal. A clear contrast difference within one composite NMI indicated the existence of a significant composition difference between the different parts in the NMI. Such differences between the contrasts were present in steels 2, 3 and 4. A larger contrast difference corresponded to a more pronounced difference in composition.

Table V. Calculated Contents of Different Components in all NMIs (g)

NMI	RE ₂ O ₂ S	RE ₂ O ₃	Slag	MnS		Total	Percent of RE NMI	
Steel 2	4.61 × 10 ⁻⁵	0.006	0.006	0.03		0.042	14 Pct	
NMI	RE ₂ S ₃	RE ₂ O ₂ S	Slag	MnS		Total	Percent of RE NMI	
Steel 3	0.012	0.023	0.002	0.015		0.052	68.2 Pct	
NMI	RE ₂ O ₂ S	Slag	MnS	TiN	Ti ₃ O ₅	Total	Percent of RE NMI	Percent of RE + Ti NMI
Steel 4	0.015	0.001	0.024	0.016	6.8 × 10 ⁻⁴	0.057	25.9 Pct	55.3 Pct

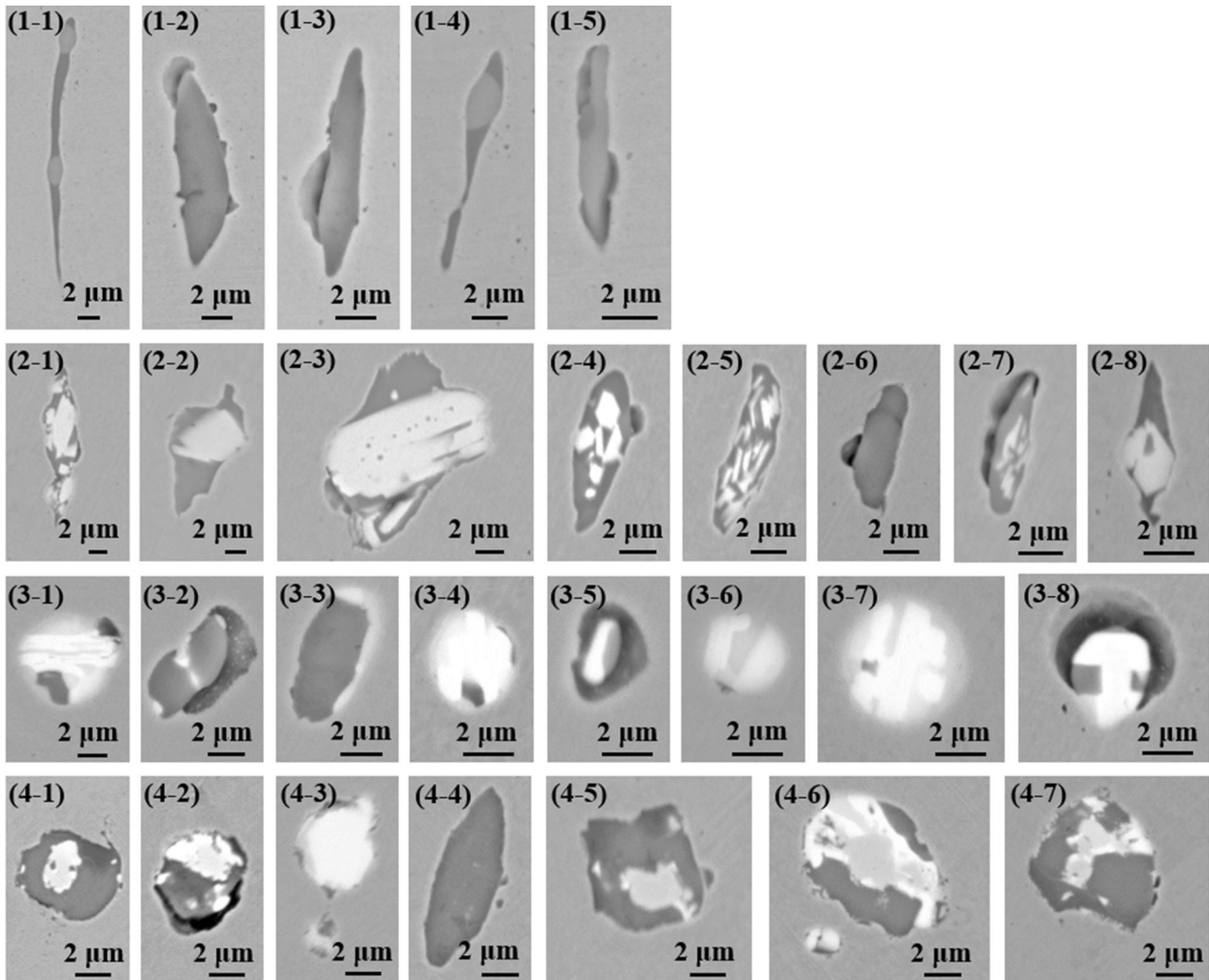


Fig. 5—Morphology of the NMIs in each sample: steel 1: (1-1) ~ (1-5); steel 2: (2-1) ~ (2-8); steel 3: (3-1) ~ (3-8); steel 4: (4-1) ~ (4-7).

When the NMIs were counted by IAA, EDS was carried out for every NMI. NMIs were distinguished by their different compositions. When the beam energy was 15 keV, the action diameter of the electron beam was approximately 1 μm. If an NMI larger than 1 μm exhibited large composition differences within the NMI, it was evaluated as more than one NMI in the IAA test process, as shown in Figure 6. For manual processing, composite NMIs with higher contrast were identified

and painted by hand one by one under backscatter mode to reduce the number of mistakes during the manual counting process.

B. Re-Analysis of the Two Methods

Based on the appearance of NMIs, in the present work, the NMIs in three RE-treated steels were divided into three categories, as shown in Figure 7. The first kind of NMI was pure RE NMIs with only white or

gray contrast. The second was RE-containing NMIs, in which a white or gray region was found within one composite NMI. These NMIs included RE NMIs and composite NMIs, which included white or gray regions. The remaining category of NMIs was comprised of NMIs with no RE at all. Therefore, all NMIs were

included in the first two kinds of NMIs and the NMIs without RE. According to this classification, the NMIs in the steel were manually re-analyzed. NMIs were manually extracted according to the NMI categories, after which Image J software was used to evaluate the area and count of the NMIs separately. The equivalent circle diameter (ECD), the diameter of a circle with the same area of the sectioned inclusion, was used to estimate the size of the NMIs.

The results regarding the size and number of NMIs obtained by manual statistics are shown in Figure 8. The fraction of the NMIs with a size of $<1 \mu\text{m}$ in the steel increased after the RE, RE-Ca and RE-Ti treatments. The mean size of the NMIs in steel 3 was only slightly smaller than that of NMIs in steel 1, while in steels 2 and 4, the mean size of the NMIs was significantly smaller. After the calcium and titanium treatments, the number densities of the NMIs in steels 3 and 4 were significantly lower than those of the NMIs in steel 2. Comparing the statistical results for number density and the mean size of the NMIs obtained with the two methods, as shown in Figure 8(c), the mean sizes of the NMIs in the RE-containing steel counted by IAA were lower than those obtained by manual statistics, and the number densities of NMIs counted by IAA were higher than those obtained by manual statistics.

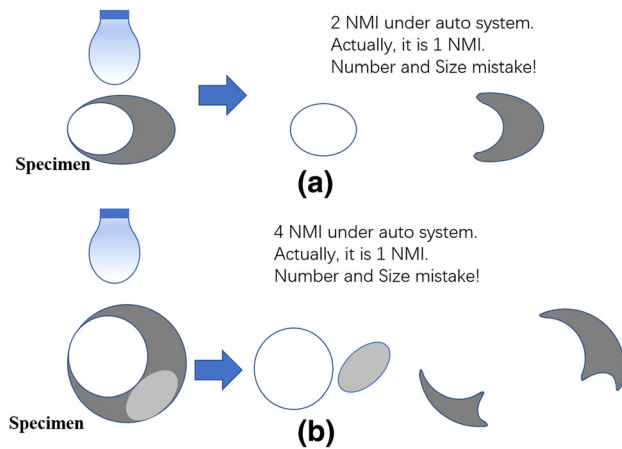


Fig. 6—Schematic diagram of the mistakes caused by EDS in IAA: (a) one composite inclusion is considered two inclusions; (b) one composite inclusion is considered more than two inclusions.

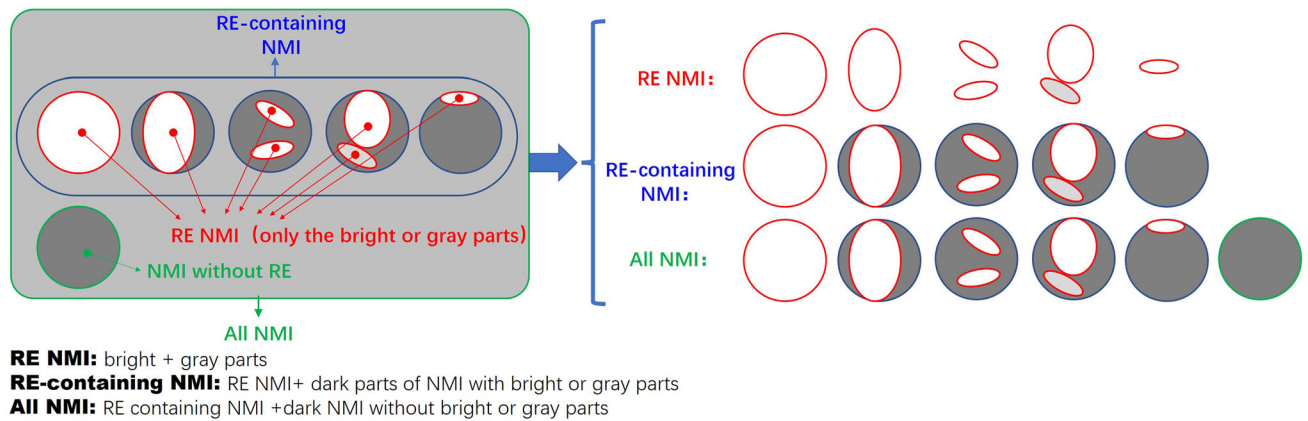


Fig. 7—Schematic diagram of NMI classification in RE-treated steels.

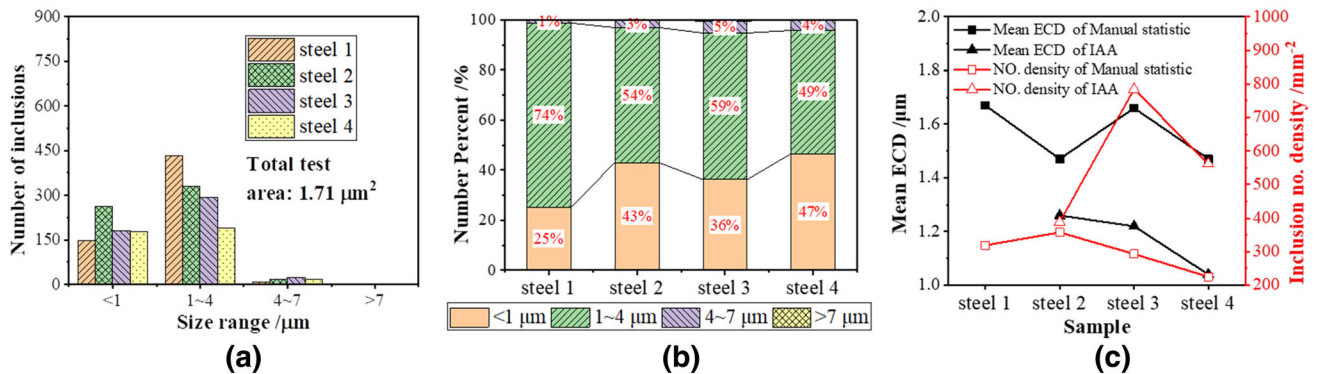


Fig. 8—Manual statistical results for the inclusions in steels. (a) NMI number; (b) Size distribution of the NMI; (c) Mean size (ECD) and number density of the NMIs.

Table VI. Comparison of the Statistical Analysis Results

Sample	Total Test Area, mm ²	S ₁		S ₂		S ₃		S ₂ /S ₁ , Pct	S ₃ /S ₁ , Pct	S ₂ /S ₃ , Pct	
		Average Value, μm ² /mm ²	Standard Deviation	Average Value, μm ² /mm ²	Standard Deviation	Average Value, μm ² /mm ²	Standard Deviation				
Auto	Steel 2	2.70	675	0.8	32	0.5	302	0.3	6.9	44.3	64.4
	Steel 3	3.53	849	0.3	741	0.9	801	0.6	80.5	94.6	85.0
	Steel 4	6.35	481	0.4	189	0.6	262	0.8	39.0	54.4	71.3
Manual	Steel 2	1.71	659	0.8	90	0.4	198	0.6	13.6	30.1	45.2
	Steel 3	1.71	917	0.7	782	0.9	872	0.4	85.3	95.1	89.7
	Steel 4	1.71	556	0.4	255	0.8	380	0.6	45.8	68.4	67.1

Note: S₁: Total area of all NMI; S₂: Total area of RE NMI (bright + gray parts); S₃: Total area of RE-containing NMI.

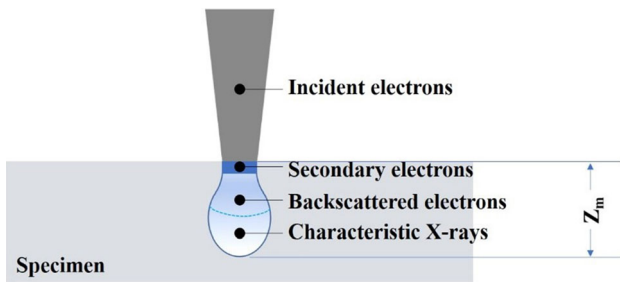


Fig. 9—Schematic diagram of the signal depths of backscattering and EDS.

Previous work has compared the two analytical methods, and it was found that for IAA, a single NMI with a large internal contrast difference could be easily misidentified as two or more NMIs by automatic analysis. The contrast of an NMI containing RE varies strongly, eventually leading to large errors in the number and size of the NMIs. This may be the very different results for the number and size of the NMIs obtained by the two methods. Therefore, manual statistical results are more reliable.

In accordance with the classification of the NMIs in Figure 7, statistical analysis was carried out again using the two methods, and the results are listed in Table VI. From the statistical results, the overall trends were found to be close, although there was a slight difference between the results with the two methods.

Generally, the action depth of EDS is approximately equal to that of the incident electrons, as shown in Figure 9. The action depth of the EDS signal in steel was approximately 1.5 μm.^[37] The action depth of the backscattered signal was only approximately 0.2 μm. From the previous statistical results, it was found that the mean sizes of the NMIs in steels 2, 3 and 4 were approximately 1.45 to 1.67 μm. The relative position between the detection depth and RE region in one NMI is shown in Figure 10. The backscattered signal could find only the RE region near the surface of the sample, as shown in Figures 10(a) and (c). However, the EDS signal action depth was greater than that of the backscattered signal. EDS could identify whether the NMIs contained RE even in the case in which no bright

region was observed under the backscattered signal, as shown in Figures 10(b) and (d). From this perspective, IAA is better than the manual statistical method. In addition, in the case in which there is a small angle between two pure RE NMI particles/plates in one composite NMI, since the action diameter of the EDS signal was too large (approximately 1 μm), the gaps between two pure RE NMI particles/plates could be mistaken for RE NMIs. Therefore, the area of the pure RE NMI particles/plates obtained by IAA may be greater than the true value, as shown in Figure 10(e). This is the origin of the larger values for IAA than for manual statistical analysis in Table V. However, it should be noted that the difference between the two statistical methods for area analysis of different kinds of NMIs was not very large. Therefore, the change trends in the area statistical results obtained by the two methods were similar, as shown in Table VI. According to the above analysis, the results obtained by both methods in counting the content and area fractions of different types of NMIs were acceptable.

C. NMI Formation

The NMI formation process has a relatively large influence on the NMI structure, in turn influencing the properties of NMIs. The statistical results for the number and area of the NMIs obtained by manual analysis are shown in Table VII. The mass percent of the RE NMIs in steel 2 and steel 3 calculated by thermodynamics in Table V were similar to the statistical number fraction and area fraction for the RE NMIs in Table VII. In particular, the calculated result was in good agreement with the statistical number fraction. In steel 2, the bright contrast region accounted for nearly half of the area of the total RE-containing NMIs, indicating that in steel 2, RE NMIs and MnS formed even, random composite NMIs. Similarly, in steel 3, the bright contrast region accounted for 89.7 pct of the total area of the RE-containing NMIs, showing that in steel 3, the amount of MnS compounded with RE NMIs was not very high. For steel 4, the calculated fraction of RE NMIs presented in Table V was much smaller than the statistical number fraction and area fraction in Table VII. However, the statistical number

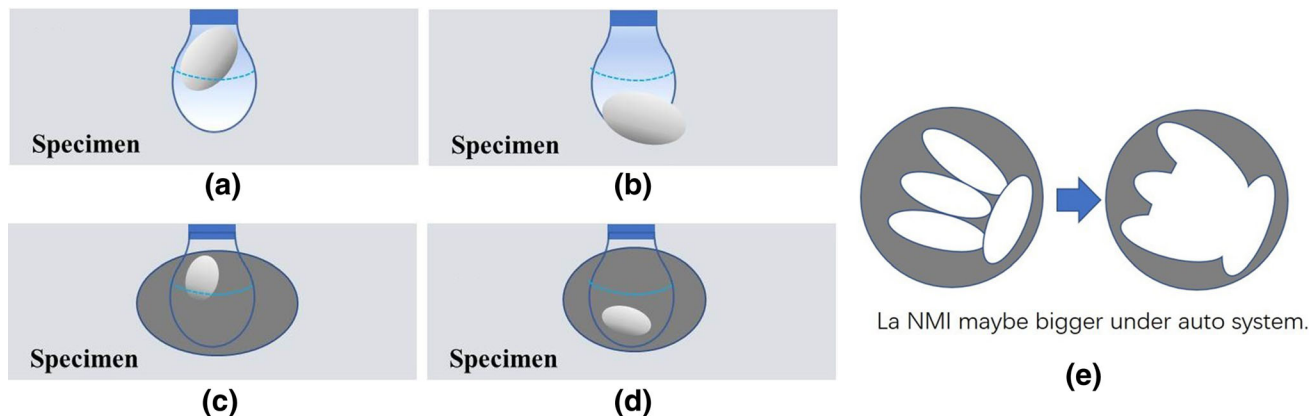


Fig. 10—Relative positions of the detection depth and the RE region in the NMI: (a) the action depths of the EDS signal and backscattered signal were greater than the distance between RE NMIs and the sample surface; (b) RE NMIs were positioned between the action depths of the EDS signal and backscattered signal; (c) the action depths of the EDS signal and backscattered signal were greater than the depth of the RE region of the RE-containing NMI; (d) position of the RE region in the RE-containing NMI was between the action depths of the EDS signal and backscattered signal; (e) the gaps between pure RE NMI particles/plates are swallowed and submerged.

Table VII. Statistical Results for NMIs Obtained by Manual Analysis

	Steel 2 (Pct)	Steel 3 (Pct)	Steel 4 (Pct)
Number Percent of RE NMI in all NMI	15.9	68.2	40.4
Area Percent of Bright Parts in All NMI	13.6	85.3	45.8
Area Percent of Bright Parts in All RE-Containing NMI	45.2	89.7	67.1

fraction of RE and area fraction of the bright regions in Table VII were similar to the fraction of RE + Ti NMIs in Table V. In steel 4, the bright contrast region accounted for 67.1 pct of the total RE-containing NMI area, implying that in steel 4, almost all Ti and RE formed composite NMIs that had more complicated structures than those in the steel after the RE and RE-Ca treatments.

V. CONCLUSION

- (1) In RE-treated steel, NMIs were refined, and the number of NMIs was increased. When calcium and titanium were combined with RE, the number densities of NMIs in the steel were reduced compared with those when only RE was added. The mean size of NMIs in the RE-Ca-treated steel was larger than that of NMIs in the RE-treated steel. For the RE-Ti-treated steel, the mean size of the NMIs was not much different from that of NMIs in the RE-treated steel. The aspect ratio of the NMIs in the RE-Ca-treated steel was the smallest, followed by the values upon RE-Ti treatment and RE treatment.
- (2) Inclusion automatic analysis may cause large errors when assessing the size and counting composite RE-containing NMIs. However, the accuracy when counting the area fraction of composite RE-containing NMIs was high. Manual statistics are a

better choice for analyzing the size and number of NMIs.

- (3) After RE treatment, RE NMI and MnS could form even, random composite NMIs. When calcium and RE were added, the amount of MnS in complex with RE NMIs was very low in composite NMIs. In RE-Ti-treated steel, the mechanism of NMI formation was complex.

ACKNOWLEDGEMENTS

This work was supported by the National Natural Science Foundations of China (NSFC) under Grant Nos. 51804229, 52074199; the Natural Science Foundations of Hubei under Grant No. 2018CFB306.

REFERENCES

1. X.Z. Gao, S.F. Yang, J.S. Li, Y.D. Yang, and K. Chattopadhyay: *Ironmaking Steelmaking*, 2018, vol. 45, pp. 611–17.
2. H.N. Lou, C. Wang, B.X. Wang, Z.D. Wang, and R.D.K. Misra: *ISIJ Int.*, 2019, vol. 59, pp. 312–18.
3. S. Lyu, X.D. Ma, Z.Z. Huang, Z. Yao, H.G. Lee, Z.H. Jiang, G. Wang, J. Zou, and B.J. Zhao: *Metall. Mater. Trans. B*, 2019, vol. 50B, pp. 732–47.
4. A. Huang, Y.Z. Huo, J.Y. Yang, H.Z. Gu, and G.Q. Li: *Minerals*, 2020, vol. 10, p. 257.

5. Y. Huang, G.G. Cheng, S.J. Li, and W.X. Dai: *Steel Res. Int.*, 2018, vol. 89, p. 1800371.
6. S. Michelic, J. Goriupp, S. Feichtinger, Y.B. Kang, C. Bernhard, and J. Schenk: *Steel Res. Int.*, 2016, vol. 87, pp. 57–67.
7. S.K. Michelic and C. Bernhard: *Scanning*, 2017, vol. 2017, pp. 1–14.
8. X.W. Zhang, L.F. Zhang, W. Yang, Y. Wang, Y. Liu, and Y.C. Dong: *Metall. Mater. Trans. B*, 2017, vol. 48B, pp. 701–12.
9. H. Wang, Y.P. Bao, M. Zhao, M. Wang, X.M. Yuan, and S. Gao: *Int. J. Miner. Metall. Mater.*, 2019, vol. 26, pp. 1372–84.
10. M.M. Song, B. Song, S.H. Zhang, Z.L. Xue, Z.B. Yang, and R.S. Xu: *ISIJ Int.*, 2017, vol. 57, pp. 1261–67.
11. M.M. Song, B. Song, C.L. Hu, W.B. Xin, and G.Y. Song: *ISIJ Int.*, 2015, vol. 55, pp. 1468–73.
12. Y. Shen, X.L. Wan, Y. Liu, G.Q. Li, Z.L. Xue, and K.M. Wu: *Ironmaking Steelmaking*, 2018, vol. 46, pp. 584–96.
13. Y.K. Yang, D.P. Zhan, H. Lei, G.X. Qiu, Z.H. Jiang, and H.S. Zhang: *ISIJ Int.*, 2019, vol. 59, pp. 1545–51.
14. Y.X. Cao, X.L. Wan, Y.H. Hou, Y. Liu, M.M. Song, and G.Q. Li: *Micron*, 2019, vol. 127, p. 102758.
15. H.L. Liu, C.J. Liu, and M.F. Jiang: *Mater. Des.*, 2012, vol. 33, pp. 306–12.
16. M. Opiela and A. Grajcar: *Arch. Foundry Eng.*, 2012, vol. 12, pp. 129–34.
17. W.G. Wilson, L.J. Heaslip, and I.D. Sommerville: *JOM*, 1985, vol. 37, pp. 36–41.
18. T.Q. He, K.M. Wu, T. Anatolii, H.W. Yu, and Y.Z. Xiong: *Wear*, 2013, vol. 303, pp. 524–32.
19. Y.X. Cao, X.L. Wan, Y.H. Hou, C.R. Niu, Y. Liu, and G.Q. Li: *Steel Res. Int.*, 2019, vol. 90, p. 1900084.
20. S. Kimura, K. Nakajima, and S. Mizoguchi: *Metall. Mater. Trans. B*, 2001, vol. 32B, pp. 79–85.
21. K.P. Wang, M. Jiang, X. Wang, W.H. Wan, and Y. Wang: *Metall. Mater. Trans. B*, 2020, vol. 51B, pp. 95–101.
22. Y.P. Chu, W.F. Li, Y. Ren, and L.F. Zhang: *Metall. Mater. Trans. B*, 2020, vol. 50B, pp. 2047–62.
23. G. Cheng, L.F. Zhang, and Y. Ren: *Ironmaking Steelmaking*, 2020, vol. 47, pp. 1217–25.
24. M. Nabeel, M. Alba, A. Karasev, P.G. Jönsson, and N. Dogan: *Metall. Mater. Trans. B*, 2019, vol. 50B, pp. 1674–85.
25. M. Alba, M. Nabeel, and N. Dogan: *Ironmaking Steelmaking*, 2020, <https://doi.org/10.1080/03019233.2020.1791549>.
26. Y. Wang, Y.X. Zhang, L.F. Zhang, N. Liu, and Y. Ren: *Steel Res. Int.*, 2020, <https://doi.org/10.1002/srin.202000605>.
27. X.L. Xin, J. Yang, Y.N. Wang, R.Z. Wang, W.L. Wang, H.G. Zheng, and H.T. Hu: *Ironmaking Steelmaking*, 2016, vol. 43, pp. 234–42.
28. Y. Luo, A.N. Conejo, L.F. Zhang, L.F. Chen, and L. Cheng: *Metall. Mater. Trans. B*, 2015, vol. 46B, pp. 2348–60.
29. C. Liu, Y. Luo, L.F. Zhang, Q. Ren, and Y. Ren: *Steel Res. Int.*, 2020, <https://doi.org/10.1002/srin.202000489>.
30. M. Alba, M. Nabeel, and N. Dogan: *Steel Res. Int.*, 2020, vol. 91, p. 1900477.
31. China Iron and Steel Association: GB/T 30834-2014 Standard test methods for rating and classifying inclusions in steel scanning electron microscope. Beijing: Standards Press of China, 2014-06-24.
32. Y.P. Chu, W.F. Li, Y. Ren, and L.F. Zhang: *Metall. Mater. Trans. B*, 2019, vol. 50B, pp. 2047–62.
33. J.H. Park and L.F. Zhang: *Metall. Mater. Trans. B*, 2020, vol. 51B, pp. 2453–82.
34. J. Janis, A. Karasev, K. Nakajima, and P.G. Jönsson: *ISIJ Int.*, 2013, vol. 53, pp. 476–83.
35. A.V. Karasev and H. Suito: *ISIJ Int.*, 2008, vol. 48, pp. 1507–16.
36. Q. Ren and L.F. Zhang: *Metall. Mater. Trans. B*, 2020, vol. 51B, pp. 589–600.
37. H. Bethe and J. Ashkin: *Experimental Nuclear Physics*, E. Serge, ed., Wiley, New York, 1953, p. 253.

Publisher's Note Springer Nature remains neutral with regard to jurisdictional claims in published maps and institutional affiliations.